metals

MDPI

Article

A Study on Heat Input Control and a Quality Evaluation Algorithm to Prevent Toughness Deterioration of the Heat-Affected Zone in the Fiber Laser Welding Process of ASTM A553-1 (9% Nickel Steel) Material

Minho Park [1], Jaewoong Kim [2,*] and Changmin Pyo [2,*]

[1] Research Institute of Medium & Small Shipbuilding, Yeongam 58457, Korea; mhpark@rims.re.kr
[2] Automotive Materials & Components R&D Group, Korea Institute of Industrial Technology, Gwangju 61012, Korea
* Correspondence: kjw0607@kitech.re.kr (J.K.); changmin@kitech.re.kr (C.P.)

Abstract: Various international organizations and governments of many countries are making efforts to prevent environmental pollution, with the IMO (International Maritime Organization) reinforcing related regulations. With these regulations, equipment related to LNG-fueled ships, which have the greatest carbon dioxide reduction effect among eco-friendly ships, are expected to increase. Although the IGC code designates the materials that can be used for LNG containers, such as 304L stainless steel and 9% nickel steel, these materials have a tendency to deteriorate the tissue around the heat-affected zone due to excessive heat input. In this study, we analyzed the effect of brittle fracture in the weld zone and heat-affected zone after fiber laser welding and found that welding quality improved with control of the heat input. SVM discriminant analysis was applied to classify the groups in which brittle fracture and ductile fracture occurred. The shape of the penetration section, hardness in the welding zone and heat-affected zone, and fracture surface were selected as factors for discrimination; these values were determined under various welding conditions. With these data, we derived a regression model and multi-objective optimization algorithm to predict mechanical properties after welding, as well as the conditions necessary to prevent brittle fracture. Finally, the prediction models were verified, as the results of welding under the derived conditions were classified as ductile fracture group.

Keywords: fiber laser welding; discriminant analysis; brittle fracture; optimization; ASTM A553-1 (9% nickel steel)

check for updates

Citation: Park, M.; Kim, J.; Pyo, C. A Study on Heat Input Control and a Quality Evaluation Algorithm to Prevent Toughness Deterioration of the Heat-Affected Zone in the Fiber Laser Welding Process of ASTM A553-1 (9% Nickel Steel) Material. *Metals* **2022**, *12*, 1195. https://doi.org/10.3390/met12071195

Academic Editor: Pasquale Russo Spena

Received: 10 June 2022
Accepted: 12 July 2022
Published: 13 July 2022

1. Introduction

With various regulations to prevent environmental pollution, orders for eco-friendly ships are increasing, and it is forecasted that LNG ships will dominate the market for the foreseeable future. Consequently, the demand for the development of ships and equipment that can reduce emission pollutants or increase energy efficiency to comply with emission regulations is accelerating. Among eco-friendly energy propulsion ships, LNG dual fuel propulsion ships are currently the most in demand and are expected to account for more than 50% of available ships by around 2035 [1–4]. LNG fuel ships should be highly reliable, and a stable supply of LNG according to the KGS AC 115 standard is a prerequisite [5,6].

The material known as 9% Ni steel is high-tensile steel generally used in the LNG condition (−160~−170 °C) after undergoing QT treatment in order to satisfy the characteristics of an LNG tank. 9% Ni steel is a material with high strength and excellent weldability. It has a high level of impact toughness at cryogenic temperatures and is more economically advantageous than stainless steel, so it is frequently used to manufacture LNG tanks. The toughness of 9% Ni steel is better than that of other metals that can be used in cryogenic conditions, although the heat-affected resistance of a weld during welding deteriorates as the heat input increases, which decreases the strength of the welding metal, so it is necessary to limit the heat input [7,8].

With respect to welding methods for 9% Ni steel, extensive research has been conducted on shield metal arc welding (SMAW), MIG welding (GMAW), TIG welding (GTAW), and submerged arc welding (SAW), through which materials suitable for each welding method have been developed. Flux-cored arc welding (FCAW) materials have been developed. With these developments, research on process optimization is required to improve product reliability. However, laser welding can minimize thermoelastic distortion, as it applies a concentrated heat source to a narrow area for a short period of time. It also increases productivity with its fast welding speed. Given these advantages, laser welding is being adopted in the industrial field, and research is being actively performed to derive welding techniques and optimal welding parameters to ensure high welding quality and less welding distortion [9–11].

Brittle fracture is a typical welding defect that can be observed in the fusion zone when welding 9% Ni steel. Such defects arise from the decline in welding quality with excessive heat input. Therefore, post-heat treatment is essential when the amount of heat input exceeds the standard range. Post-heat treatment may work effectively in the redistribution of welding residual stress, but it may lead to a decrease in toughness, and heat treatment is not possible for a large-sized product. For this reason, it is urgent to secure the safety of a structure through the accurate toughness evaluation of a weld under actual field conditions. With the recent increase in demand for 9% Ni steel, basic research on the possibility of brittle fracture with excessive welding heat input is required.

Therefore, in this study, we analyzed the brittle fracture characteristics that can take place during the fiber laser welding process with 9% Ni cryogenic steel used to produce LNG storage tanks. The aim of this study was to establish the brittle effect and quality deterioration criteria due to excessive heat input and suggest the optimal process variables to identify the appropriate range of heat input.

2. Experimental Works

9% Ni steel (thickness: 15 mm) was used for this study. The chemical composition is indicated in Table 1, and the principal mechanical properties are shown in Table 2.

Table 1. Chemical composition of steels used (wt. %).

Steel	C	Si	Mn	S	P	Ni	Fe
A553-1	0.05	0.67	0.004	0.003	0.25	9.02	Bal.

Table 2. Mechanical properties of steels used.

Steel	Yield Strength (MPa)	Tensile Strength (MPa)	Elongation (%)	Hardness (HV)
A553-1	651.6	701.1	26.6	243

Bead-on-plate welding was conducted with 4 point constraints, as described in Figure 1. Additionally, the whole welding surface was cleaned using ethyl alcohol and sand paper before welding.

In this experiment, 100% Ar was used as a shielding gas for welding; the fiber laser welding device is shown in Figure 2. The systems used in this experiment were a 5kW-class fiber laser welding machine (MIYACHI ML-6950A, Amada Weld Tech Co. Ltd., Chiba, Japan) and a welding torch head (YASKAWA DX100 model MOTOMAN, Yaskawa Electric Co., Kitakyushu, Japan).

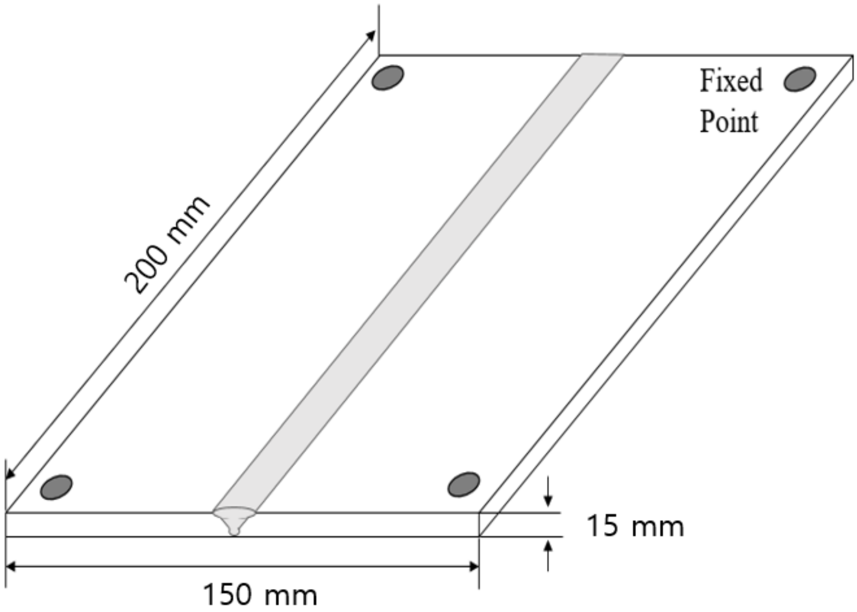

Figure 1. Schematic diagram of the welding specimen and constraints.

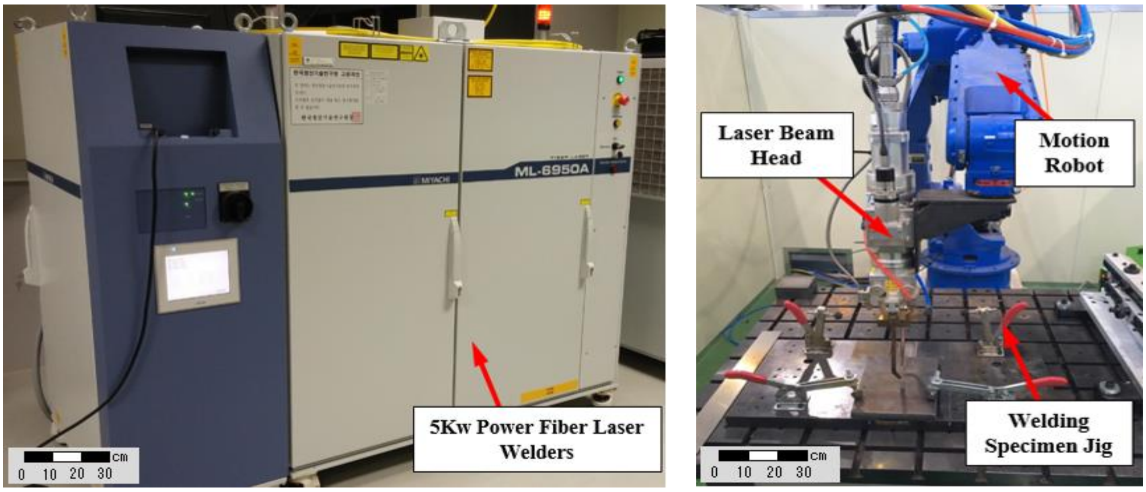

(**a**) (**b**)

Figure 2. Fiber laser welding equipment. (**a**) 5kw fiber laser power source; (**b**) welding torch head.

The input conditions for the fiber laser welding experiment comprised the laser power, focal length, and welding speed, which can influence the penetration shape and welding quality. Furthermore, the penetration shape, impact amount, and the fracture surface were chosen to judge the weldability.

Figure 3 shows a schematic diagram of the measurement parameters of the penetration shape of a weld [12]. Full factorial design, which can predict all the factor effects of the measured data response by input conditions and maximize the interaction effect of higher orders, was used for this experiment. The following appropriate ranges were selected through preliminary experiments as input variables: a laser power of 3.0~5.0 kW, a focal length of −0.5~0.5 mm, and a welding speed of 0.5~0.8 m/min. A total of 18 (9 × 2) experimental conditions were generated. Table 3 indicates the experimental conditions of fiber laser welding.

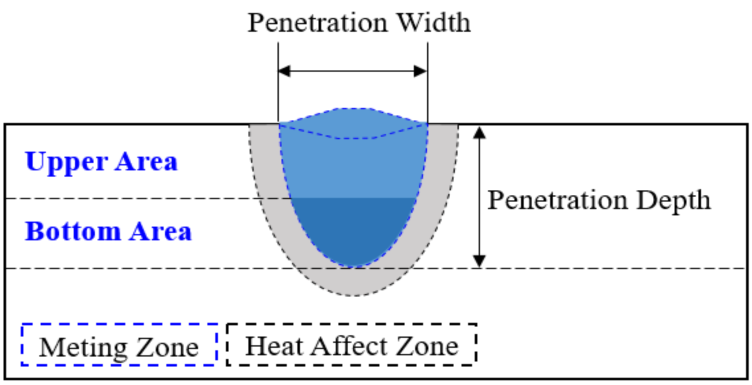

Figure 3. Schematic diagram of penetration geometry measurement.

Table 3. Fiber laser welding parameters and experimental conditions.

Test No.	Laser Power (kW)	Defocusing (mm)	Welding Speed (m/min)	Test No.	Laser Power (kW)	Defocusing (mm)	Welding Speed (m/min)
1	3.0	−0.5	0.5	10	3.0	−0.5	0.8
2	3.0	0.0	0.5	11	3.0	0.0	0.8
3	3.0	0.5	0.5	12	3.0	0.5	0.8
4	4.0	−0.5	0.5	13	4.0	−0.5	0.8
5	4.0	0.0	0.5	14	4.0	0.0	0.8
6	4.0	0.5	0.5	15	4.0	0.5	0.8
7	5.0	−0.5	0.5	16	5.0	−0.5	0.8
8	5.0	0.0	0.5	17	5.0	0.0	0.8
9	5.0	0.5	0.5	18	5.0	0.5	0.8
Fixed Parameter				Wavelength: 1070 nm Optical Fiber Diameter: 200 µm Shielding Gas Flow Rate: 18 L/min, (L/min)			

3. Results of Fiber Laser Welding

3.1. Measurement of Penetration Geometry

Proper penetration was made on the surface and cross section of a test piece for each process parameter, and no pores or defects were observed in the 9% Ni steel, which is a cryogenic steel. To assess the cross-sectional shape of the weld, an etching solution (90% ethanol + 10% nitric acid) was mixed, and the shape of the weld was measured using an optical microscope system after the etching solution was applied on the cross section. The penetration shape and measurement results obtained from the optical microscope are shown in Table 4.

3.2. Measurement of Impact Energy

A Charpy impact test was conducted on each specimen to understand the deformation and fracture processes of the weld and to apprehend the quality and fracture characteristics of the weld based on the measured toughness. The factors that affect the impact value of a material include the material type, grains in microstructures, and the impact speed. The material toughness was measured after opening a notch in the heat-affected zone of the Charpy specimen. For measurement, a length of 55 mm and a square cross section of 10 mm × 10 mm were created, and a V-shaped notch with a depth of 2 mm a notch angle of 45° was applied according to ASTM E 23-02. Figure 4 presents schematic diagram of the specimen for the Charpy impact test.

Table 4. Results of penetration geometry through welding experiment.

Test No.	Penetration Width (mm)				Penetration Depth (mm)				Penetration Geometry
	1st	2nd	3rd	Average	1st	2nd	3rd	Average	
1	3.93	3.90	3.90	3.91	6.49	6.47	6.51	6.49	
2	3.19	3.18	3.17	3.18	6.64	6.66	6.64	6.65	
3	4.73	4.72	4.69	4.71	7.21	7.22	7.15	7.19	
4	5.82	5.86	5.84	5.84	8.52	8.51	8.55	8.53	
5	5.48	5.49	5.49	5.49	8.17	8.15	8.15	8.16	
6	3.61	3.71	3.5	3.61	7.84	7.82	7.79	7.82	
7	6.59	6.58	6.58	6.58	9.11	9.12	9.11	9.11	
8	6.54	6.55	6.55	6.55	9.49	9.51	9.53	9.51	
9	7.01	7.03	7.04	7.03	10.09	10.09	10.11	10.1	
10	2.51	2.47	2.37	2.45	4.86	4.78	4.79	4.81	
11	2.21	2.28	2.32	2.27	4.95	4.89	4.95	4.93	
12	3.26	3.27	3.22	3.25	5.19	5.23	5.21	5.21	
13	3.25	3.23	3.17	3.22	5.49	5.48	5.44	5.47	
14	3.22	3.30	3.20	3.24	6.25	6.24	6.29	6.26	
15	2.82	2.84	2.86	2.84	5.43	5.44	5.54	5.47	
16	4.94	4.97	4.91	4.94	6.18	6.24	6.21	6.21	
17	4.25	4.19	4.21	4.22	7.26	7.24	7.24	7.25	
18	5.84	5.83	5.85	5.84	7.47	7.41	7.44	7.44	

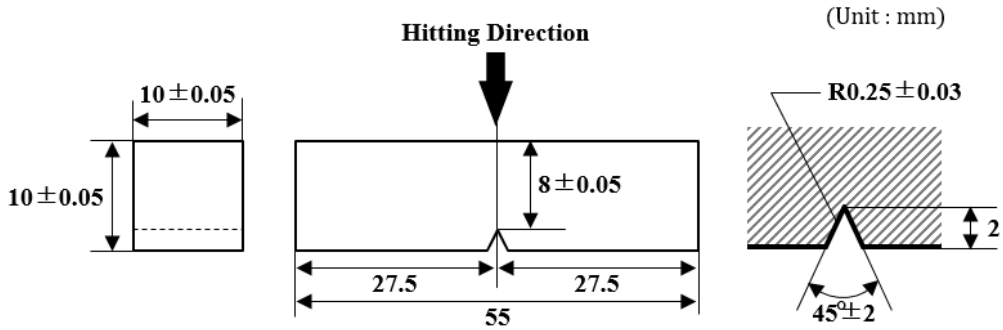

Figure 4. Schematic diagram of the Charpy impact test.

In the Charpy impact test, the specimen fractures due to a momentary load from 1×10^{-3} to 5×10^{-5} s, and the material strength is calculated based on the amount of energy required for this failure. The impact tester used in the experiment can produce an impact of up to 300 J of maximum impact energy and the height of a weight that rises to the opposite side is determined by the energy excluding the energy used to break the specimen. Based on this, the impact energy per unit area used to break the specimen can be calculated. Therefore, the impact amount was calculated by multiplying the energy per unit area used for the fracture of the Charpy impact specimen by the specimen's fracture area.

The impact toughness of a heat-affected zone in the specimen welded in accordance with each process was examined, and an impact amount of 34 J or more, which is the standard condition for cryogenic steel, was confirmed throughout the entire experiment, verifying the weldability applicable to a product operating at cryogenic temperatures. The results are shown in Tables 5 and 6.

Table 5. Results of Charpy impact test according to fiber laser welding.

Test No.	1st (J)	2nd (J)	3rd (J)	Average (J)
1	70.46	69.54	70.71	70.24
2	69.92	68.72	67.87	68.84
3	74.89	72.16	72.36	73.14
4	42.86	44.12	44.76	43.91
5	45.97	42.14	44.92	44.34
6	58.56	57.12	56.89	57.52
7	65.42	62.16	61.91	63.16
8	42.71	44.56	43.87	43.71
9	48.09	46.21	47.02	47.11
10	69.08	65.21	66.84	67.04
11	66.41	63.12	68.33	65.95
12	73.71	71.69	72.52	72.64
13	70.36	68.50	68.44	69.10
14	67.62	66.12	68.24	67.33
15	68.23	68.91	68.12	68.42
16	73.41	68.83	72.64	71.63
17	54.96	48.22	51.26	51.48
18	72.12	71.60	71.01	71.58

Table 6. Results of fracture geometry of the heat-affected zone according to the Charpy impact test.

Test No.					
Facets					
1	2	3	4	5	6
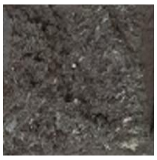		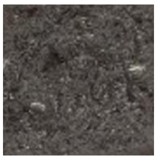	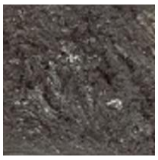	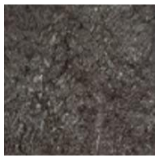	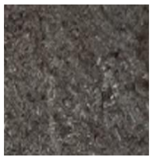
7	8	9	10	11	12
	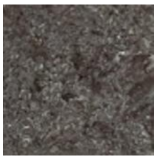	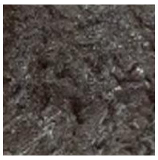	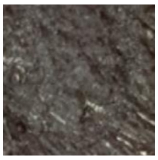		
13	14	15	16	17	18
		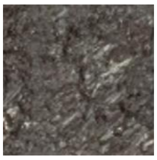	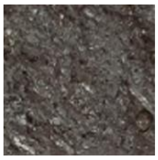	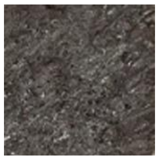	

3.3. Analysis of Brittle Fracture of Heat-Affected Zone

A brittle fracture can occur even under a typically acceptable low load, and a crack can develop instantaneously, often causing fatal structural damage. Among a variety of destruction phenomena, this is the most dangerous type of destruction that can occur in relation to structural machinery and equipment, possibly triggering a large-scale accident [13,14]. With respect to steel, the growth speed of a brittle crack can reach up to 2000 m per second. Therefore, a study to identify whether a brittle force applies or not depending on the mechanical properties or chemical composition of a weld is urgently required. The valuable information that can be obtained directly from the fracture surface in a Charpy impact test for the heat-affected zone is largely categorized into two types. The first piece of information concerns whether the fracture is a ductile fracture or a brittle fracture, and the second piece of information concerns where a crack starts and propagates. In this study, we excluded analysis of crack initiation because crack initiation induces fractures by opening a notch. As shown in Figure 5, in the case of ductile fracture, a fracture surface is created like a tear, and a brittle fracture includes the characteristics of a flat fracture surface, so the influence that the ductility and the degree of brittleness can exert was determined based on such a fracture surface.

The plastic deformation formed on a fracture surface takes the form of a brittle cleavage because the structure becomes rigid as a result of the generation of impure fine particles, such as oxides, carbides, nitrides, etc., inherent in the material and due to excessive heat input. Therefore, in this study, as shown in Figure 6, the influence of brittle fracture per welding process variables and heat input was analyzed after confirming the fracture type using SEM (scanning electron microscopy) at the analysis location where the cracking of a fractured impact specimen begins.

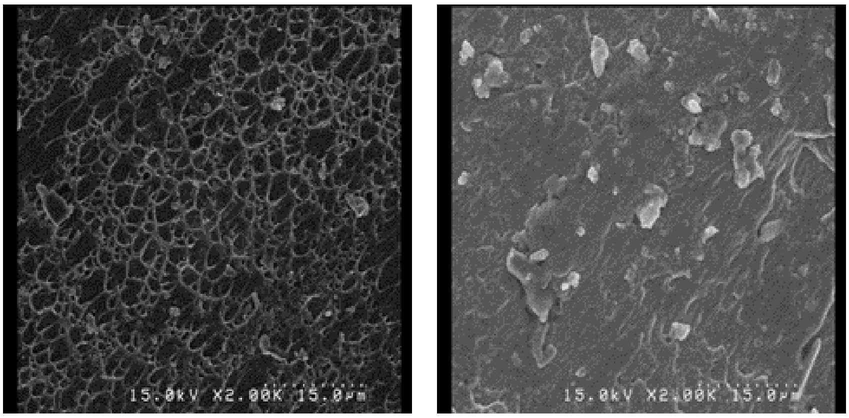

Figure 5. Typical fracture surface according to ductility and brittleness. (**a**) Ductile fracture; (**b**) brittle fracture.

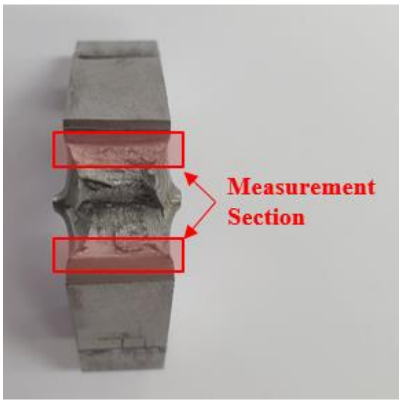

Figure 6. Definition of measurement section for impact specimens.

In general, the shape of fractures can be divided into cleavage fractures and dimple fractures. When a cleavage fracture is generated based on the two fracture shapes, it is called a brittle fracture, and it is called a ductile fracture when a dimple fracture is created. These categories were named in prior studies and used as the basis for a theory to predict fracture behavior. Table 7 shows the fracture behavior of a heat-affected zone of 9% Ni steel, which is a cryogenic steel, based on such fracture surface determination criteria [15,16].

Table 7. Results of fracture geometry analysis of the heat-affected zone according to the Charpy impact test.

Test No.					
Facets					
1	2	3	4	5	6
Dimple	Dimple	Dimple	Cleavage	Cleavage	Dimple
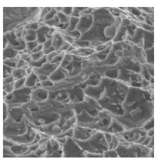	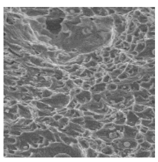	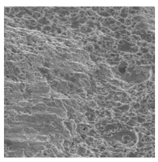	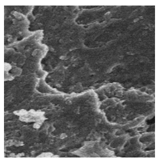	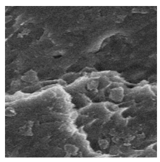	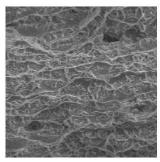

Table 7. *Cont.*

Test No.					
Facets					
7	8	9	10	11	12
Dimple	Cleavage	Cleavage	Dimple	Dimple	Dimple
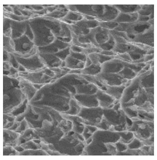	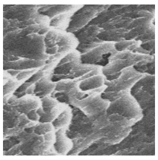	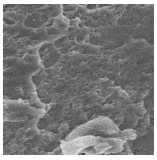	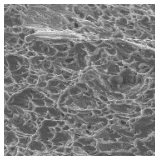	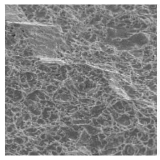	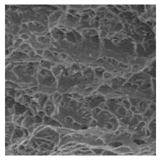
13	14	15	16	17	18
Dimple	Dimple	Dimple	Dimple	Cleavage	Dimple
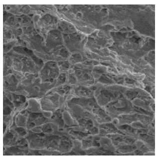	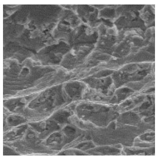	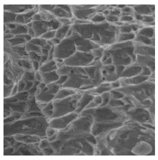	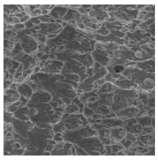	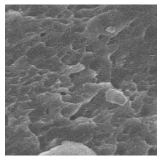	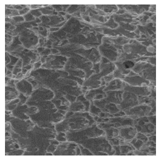

4. Discussion

4.1. Brittle Fracture Behavior

Several studies have been conducted on alloying elements, as well as the effect of cooling rate and texture on weld toughness, but basic research on cryogenic welding steel developed to date and welding conditions, such as in relation to high efficiency and high adhesion, is lacking. In line with the recent increase in demand for 9% Ni steel used to produce LNG storage tanks, basic research on the possibility of brittle fracture due to excessive welding heat input is required [17,18].

To analyze the brittleness of 9% Ni steel as part of the basic research mentioned above, a Charpy impact test was performed based on the welding process and process variables necessary to cause a fracture to a specimen. The correlation between the cross section of the fractured specimen and the amount of heat input from the welding was determined in order to define an appropriate range of heat input. To assess the brittleness of the weld, the fracture behavior results collected from the fractured section during the heat-affected zone impact test were used, and Formula (1) was employed with regard to the amount of heat input applied to each weld.

$$H_i = P(w \cdot v)^{-1} \tag{1}$$

where H_i is the heat input of fiber laser welding, P is laser power (kW), w is penetration width (mm), and v is torch speed (cm/min). The heat input results according to the welding process and process variables are presented in Table 8, and the factors necessary for heat input calculation and the fracture behavior results are also included.

To analyze the brittle force of 9% Ni steel, which is a cryogenic steel, the distribution between the Charpy impact test result and the welding heat input was verified to determine an appropriate range of heat input to be applied to the weld. As a result of analysis, we found that the heat input was in the range of 6.42×10^7~1.33×10^8 J/cm^2. Although the heat input range of fiber laser welding includes a sufficient amount of impact in comparison to the base material, it can be ascertained that brittle force in the form of a cleavage fracture was applied due to the decrease in toughness caused by an excessive heat input and tissue hardening. As shown in Figure 7, when the arc heat input was in the range of 8.22×10^7~9.16×10^7 J/cm^2, it was determined that the shock amount started at 51.48 J and decreased to 43.71 J, meaning that brittleness occurred in the form of a cleavage fracture. Fracture surface analysis can determine, in advance, the brittle action on the weld and heat-affected zone according to the process variables and can serve as data to avoid the suggested range and secure the weld toughness.

Table 8. Results of fracture behavior according to heat input in fiber laser welding.

Test No.	Laser Power (kW)	Defocusing (mm)	Welding Speed (m/min)	Penetration Width (mm)	Penetration Depth (mm)	Heat Input (J/cm^2)	Impact Energy (J)	Fracture Behavior
1	3.0	−0.5	0.5	3.91	6.49	9.21×10^7	70.24	Dimple
2	3.0	0.0	0.5	3.18	6.65	1.13×10^8	68.84	Dimple
3	3.0	0.5	0.5	4.71	7.19	7.64×10^7	73.14	Dimple
4	4.0	−0.5	0.5	5.84	8.53	8.22×10^7	43.91	Cleavage
5	4.0	0.0	0.5	5.49	8.16	8.74×10^7	44.34	Cleavage
6	4.0	0.5	0.5	3.61	7.82	1.33×10^8	57.52	Dimple
7	5.0	−0.5	0.5	6.58	9.11	9.12×10^7	63.16	Dimple
8	5.0	0.0	0.5	6.55	9.51	9.16×10^7	43.71	Cleavage
9	5.0	0.5	0.5	7.03	10.1	8.55×10^7	47.11	Cleavage
10	3.0	−0.5	0.8	2.45	4.81	9.18×10^7	67.04	Dimple
11	3.0	0.0	0.8	2.27	4.93	9.91×10^7	65.95	Dimple
12	3.0	0.5	0.8	3.25	5.21	6.92×10^7	72.64	Dimple
13	4.0	−0.5	0.8	3.22	5.47	9.35×10^7	69.10	Dimple
14	4.0	0.0	0.8	3.24	6.26	9.26×10^7	67.33	Dimple
15	4.0	0.5	0.8	2.84	5.47	1.06×10^8	68.42	Dimple
16	5.0	−0.5	0.8	4.94	6.21	7.59×10^7	71.63	Dimple
17	5.0	0.0	0.8	4.22	7.25	8.91×10^7	51.48	Cleavage
18	5.0	0.5	0.8	5.84	7.44	6.42×10^7	71.58	Dimple

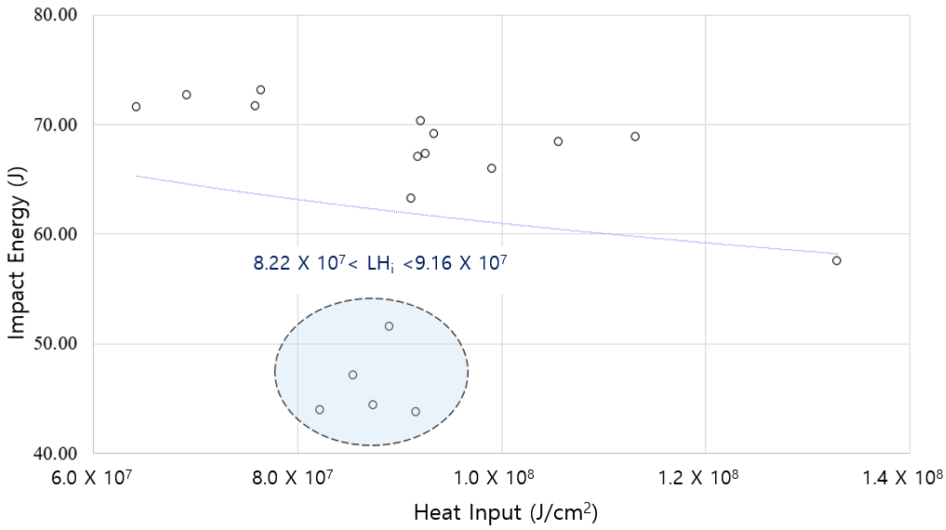

Figure 7. Impact energy distributions according to heat input in fiber laser welding.

The criterion for the amount of heat input, i.e., (8.22×10^7~9.16×10^7) J/cm^2, of the brittle fracture characteristic described above is a quality deterioration determination score. It can be employed to evaluate the weldability of the welding process and is an indicator of whether a brittle fracture can take place when the heat input is located within a specific range, leading to the brittle facture determination criteria shown in Table 9. These quality deterioration determination scores can be developed and availed of as learning data to determine the brittle effect and fracture caused by heat input and can also be utilized as important data to avoid the problem of toughness degradation due to excessive welding residual stress in 9% Ni steel welds when fiber laser welding is applied.

Table 9. Brittle fracture behavior data for discriminant analysis in fiber laser welding.

Test No.	Heat Input (J/cm^2)	Impact Energy (J)	Fracture Behavior	Test No.	Heat Input (J/cm^2)	Impact Energy (J)	Fracture Behavior
1	9.21×10^7	70.24	Dimple	10	9.18×10^7	67.04	Dimple
2	1.13×10^8	68.84	Dimple	11	9.91×10^7	65.95	Dimple
3	7.64×10^7	73.14	Dimple	12	6.92×10^7	72.64	Dimple
4	8.22×10^7	43.91	Cleavage	13	9.35×10^7	69.10	Dimple
5	8.74×10^7	44.34	Cleavage	14	9.26×10^7	67.33	Dimple
6	1.33×10^8	57.52	Dimple	15	1.06×10^8	68.42	Dimple
7	9.12×10^7	63.16	Dimple	16	7.59×10^7	71.63	Dimple
8	9.16×10^7	43.71	Cleavage	17	8.91×10^7	51.48	Cleavage
9	8.55×10^7	47.11	Cleavage	18	6.42×10^7	71.58	Dimple

4.2. Discriminant Analysis

The 9% Ni steel welding quality determination system utilized in this study employs a technique to determine a group through quantitative evaluation of data by devising a mathematical model based on the collected data and learning the characteristic data between groups. Therefore, the purpose of this study was to specify a criterion that can help determine the quality of the process by learning the welding quality results between the input and output variables obtained from the welding process. In general, the welding process has many variables and is a multivariate process with numerous interactions, such as mechanical strength and fracture characteristics occurring depending on the process variables. Thus, a high-accuracy discrimination technique must be adopted through the application of various techniques. Here, accuracy signifies an index that can quantitatively confirm the extent to which the actual group and the group classified by the model match when classifying data based on discriminant analysis [19–21].

To determine the quality of the process, the process data were learned using the SVM technique. SVM (support vector machine) is an algorithm created by Vapnik in 1995. Based on the VC (Vapnik–Chervonenkis) theory, SVM was developed in order to resolve the problem of finding the hyperplane, $w \cdot x + b = 0$, that differentiates two classes while supporting linear separation and maximizing the margin [22].

Here, w is a weight vector, x is an input vector, and b is a reference value. The SVM technique involves sequentially performing minimal optimization of complex calculations in the QP (quadratic programming) process. The SVM is fundamentally a classifier specialized in classifying two categories. Finally, the closest data of each group are referred to as a support vector, and an optimal separation boundary is set at the point where the distance between the support vectors of each group is maximized to classify the belonging group.

The variables deployed for learning in regard to the brittle fracture characteristics determination model are welding process parameters (laser power, defocusing, and welding speed), penetration shape (penetration width and penetration depth), heat input, impact energy, and fracture behavior. A total of 144 data items were input with 8 variables. In order to determine the brittle fracture characteristics, the cleavage group was defined as 1, and the dimple group was defined as 0. The accuracy was verified by reviewing whether the group predicted by the SVM method was discriminated in an identical manner identical with regard to the actual group.

Table 10 shows the training data used to discriminate brittle fracture characteristics, and Table 11 and Figure 8 quantitatively present the discrimination performance of fracture characteristic groups predicted by the data learned through the SVM technique.

Table 10. Learning data for discrimination of welding quality.

Test No.	L	D	S	P_W	P_D	H_i	I	Group
1	3.0	−0.5	0.5	3.91	6.49	9.21×10^7	70.24	Dimple
2	3.0	0.0	0.5	3.18	6.65	1.13×10^8	68.84	Dimple
3	3.0	0.5	0.5	4.71	7.19	7.64×10^7	73.14	Dimple
4	4.0	−0.5	0.5	5.84	8.53	8.22×10^7	43.91	Cleavage
5	4.0	0.0	0.5	5.49	8.16	8.74×10^7	44.34	Cleavage
6	4.0	0.5	0.5	3.61	7.82	1.33×10^8	57.52	Dimple
7	5.0	−0.5	0.5	6.58	9.11	9.12×10^7	63.16	Dimple
8	5.0	0.0	0.5	6.55	9.51	9.16×10^7	43.71	Cleavage
9	5.0	0.5	0.5	7.03	10.1	8.55×10^7	47.11	Cleavage
10	3.0	−0.5	0.8	2.45	4.81	9.18×10^7	67.04	Dimple
11	3.0	0.0	0.8	2.27	4.93	9.91×10^7	65.95	Dimple
12	3.0	0.5	0.8	3.25	5.21	6.92×10^7	72.64	Dimple
13	4.0	−0.5	0.8	3.22	5.47	9.35×10^7	69.10	Dimple
14	4.0	0.0	0.8	3.24	6.26	9.26×10^7	67.33	Dimple
15	4.0	0.5	0.8	2.84	5.47	1.06×10^8	68.42	Dimple
16	5.0	−0.5	0.8	4.94	6.21	7.59×10^7	71.63	Dimple
17	5.0	0.0	0.8	4.22	7.25	8.91×10^7	51.48	Cleavage
18	5.0	0.5	0.8	5.84	7.44	6.42×10^7	71.58	Dimple

L: laser power (kW); D: defocusing (mm); S: welding speed (m/min); P_W: penetration width (mm); P_D: penetration depth (mm); H_i: heat input (J/cm^2); I: impact energy (J).

Table 11. Results of group discrimination for brittle fracture behavior according to SVM.

Test No.	Measured Group	Predicted Group	Test No.	Measured Group	Predicted Group
1	0	0 (0.00)	10	0	0 (0.00)
2	0	0 (0.00)	11	0	0 (0.00)
3	0	0 (0.00)	12	0	0 (0.00)
4	0	0 (0.00)	13	0	0 (0.00)
5	1	1 (1.00)	14	0	0 (0.00)
6	1	1 (1.00)	15	0	0 (0.00)
7	1	1 (1.00)	16	0	0 (0.00)
8	1	1 (1.00)	17	0	0 (0.00)
9	1	1 (1.00)	18	0	0 (0.00)

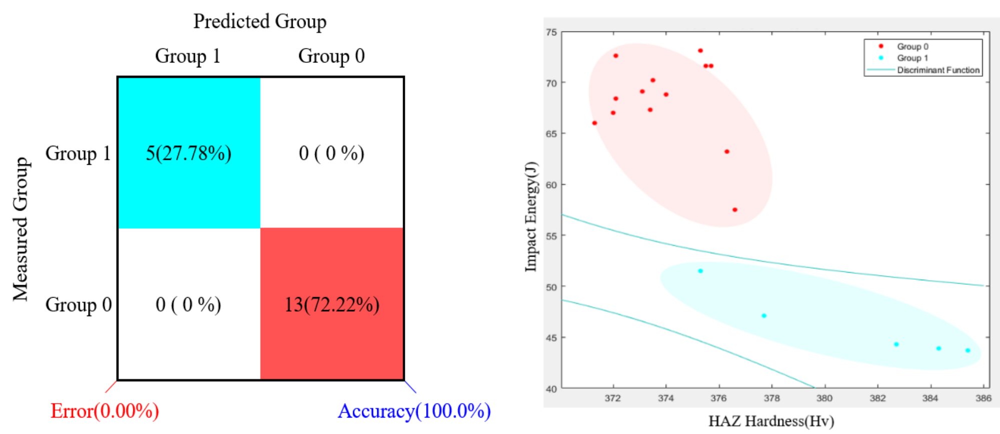

(**a**) (**b**)

Figure 8. Brittle fracture behavior discrimination in fiber laser welding: (**a**) performance evaluation for SVM and (**b**) discrimination graph for SVM.

5. Optimization of Fiber Laser Welding of 9% Ni Steel

5.1. Development of Mathematical Model Welding Parameters

Regression analysis is one of the analysis methods by which to assess the quantitative relationship between cause and effect or effect and effect. Because the welding process variables significantly impact welding quality, this analysis method can mathematically illustrate the correlation between input and output factors. When welding quality is affected by different factors in a complex manner, several independent variables ($x_1,\ x_2, x_3,\ \ldots x_k$) are prepared, and one dependent variable, i.e., welding quality (y), can be explained in a regression equation as formulated in Equation (2). By reflecting the factor calculation capability of linear and nonlinear models, the predicted values of welding factors can be expressed as a second-order linear regression model by assuming a linear relationship with the input variables.

$$Y_i = \beta_0 + \sum_{i=1}^{k} \beta_i k_i + \sum_{i\leq j}^{k} \beta_{ij} x_i x_j + \epsilon \tag{2}$$

Equation (2) can be reformulated as Equation (3) by the least squares method.

$$\hat{Y}_i = \hat{\beta}_i + \sum_{i=1}^{k} \hat{\beta}_i k_i + \sum_{i\leq j}^{k} \hat{\beta_{ij}} x_i x_j + c \tag{3}$$

In this study, Equation (3) can be expanded as Equation (4), as there are three input variables (k = 3).

$$\begin{aligned} \hat{Y}_i = \hat{\beta_0} + \hat{\beta_1} x_1 + \hat{\beta_2} x_2 + \hat{\beta_3} x_3 + \hat{\beta_{11}} x_1^2 + \hat{\beta_{22}} x_2^2 + \hat{\beta_{33}} x_3^2 \\ + \hat{\beta_{12}} x_1 x_2 + \hat{\beta_{13}} x_1 x_3 + \hat{\beta_{23}} x_2 x_3 \end{aligned} \tag{4}$$

Here, $\hat{Y}_i$ is the predicted quantity of welding factors; x_i is the code unit of welding process variables and mechanical strengths; $\hat{\beta_0},\ \hat{\beta_i},\ \hat{\beta_{ij}}$ are the least-squares estimators of $\beta_0,\ \beta_i,\ \beta_{ij}$, respectively; and ϵ represents the error. To develop a second-order regression model, data must be attained from many experiments. However, there may be some experimental errors, as well as a loss of time and money. Therefore, the response surface analysis method was implemented to address this issue [23].

The mathematical prediction model of the penetration shape (penetration width and depth) and impact energy developed using the regression coefficient and Equation (4) can be expressed as Equations (5)–(7).

$$P_W = 8.871 - 2.537L - 1.354D - 2.463S + 0.5375L^2 + 1.440D^2 \tag{5}$$

$$- 0.06251LD - 0.7389LS + 2.556DS$$

$$P_D = 5.651 + 1.089L - 1.154D - 2.174S + 0.1233L^2 - 0.5567D^2 \tag{6}$$

$$+ 0.2800LD - 1.356LS + 0.7222DS$$

$$I\ = 560.5 - 433.9S + 67.98P_W - 132.3P_D + 12.96P_W^2 \tag{7}$$

$$+ 10.48P_D^2 - 51.89SP_W + 89.82SP_D - 20.005P_W P_D$$

To assess the performance of the mathematical model to predict quality factors derived from the welding process, the average value of welding factors actually measured in each test was compared with the predicted welding factors. The error range is shown in Figure 9. In addition, Table 12 displays the quantitative performance evaluation of the mathematical model. An ANOVA of the mathematical model revealed the highest coefficient of determination for penetration depth with a coefficient of determination of 96.3%, and the minimum coefficient of determination of 75.6% was obtained with the impact energy of the heat-affected zone. This result of coefficient of determination can predict welding quality close to the coefficient of determination for the changes in welding process variables and reflects the independence and interaction of factors affecting the regression model.

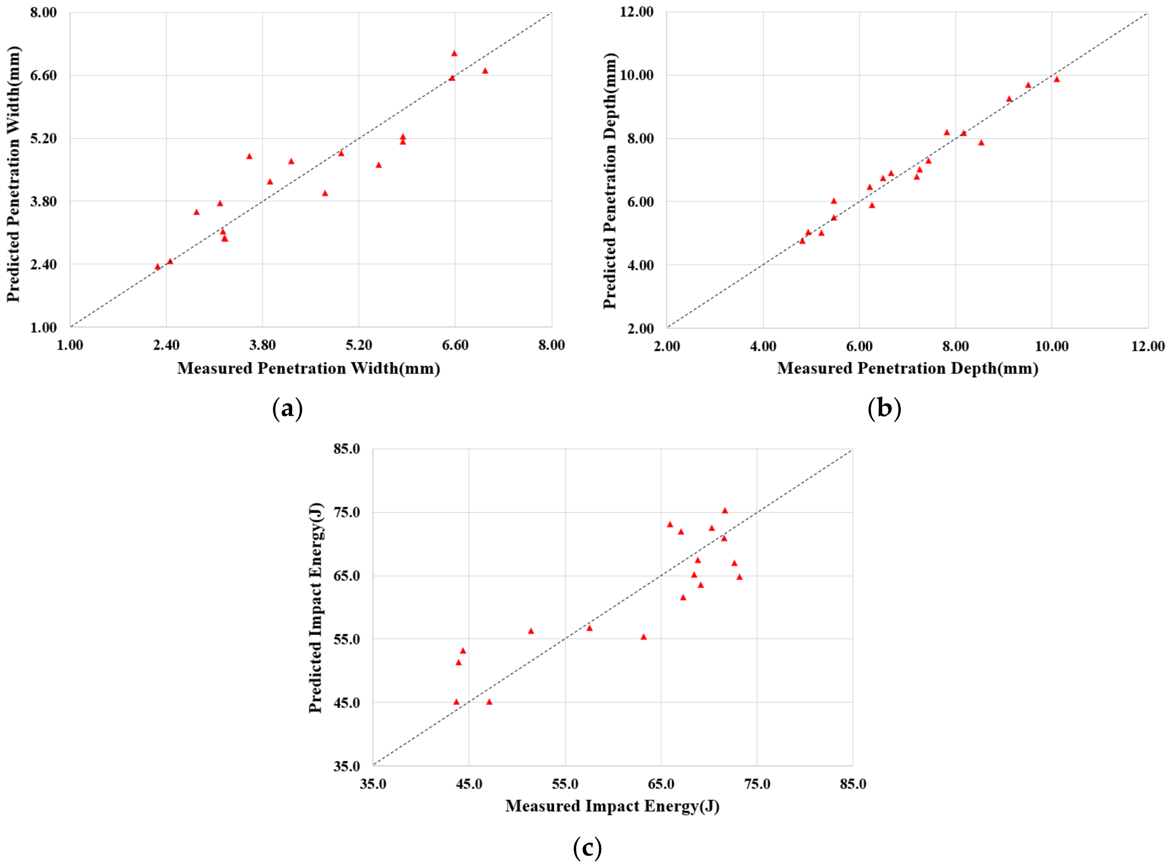

Figure 9. Comparison between measured and predicted welding factors according to mathematical model: (**a**) penetration width, (**b**) penetration depth, (**c**) impact energy.

Table 12. Analysis of variance tests for predicted model for welding factors.

Design Parameter	Predicted Model	SE (Standard Error)	R^2 (Coefficient of Determination, %)
P_W	Response Surface Analysis	0.769	86.4
P_D	Response Surface Analysis	0.423	96.3
I	Response Surface Analysis	7.411	75.6

5.2. Optimization for Welding Process of 9% Ni Steel

Multi-objective optimization, as employed in this study, is a technique used to search for a non-dominant solution by imitating the evolutionary process of an organism in an optimization problem with multiple objectives. By comparing and evaluating non-dominant solutions obtained from multi-purpose genetic algorithms, tradeoffs between objective functions can be determined, and ultimately, an optimal solution can be effectively attained. Owing to these advantages, multi-purpose genetic algorithms have garnered much attention as a technique to deal with a multi-purpose optimization problem in engineering, natural science, business administration, and social sciences [24]. The main purpose of an optimization algorithm is to identify various appropriate solutions, which means convergence to the Pareto optimal solution set and diversity, indicating a uniform distribution of solutions. For the widespread use of multi-purpose algorithms, the weight and population of multi-objective functions are operated in various ways to evaluate the fitness, and the selection operation is performed to repeat the generation. Performance depends on the number of iterations and convergence time. Based on this theorem, the schematic diagram of the MOO optimization method is presented in Figure 10.

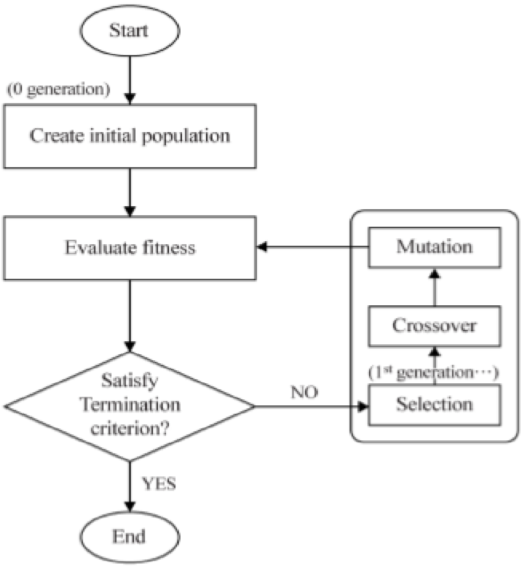

Figure 10. Flow chart for the MOO method to predict welding parameters.

The multipurpose optimization problem can be outlined as in Equation (8) below.

$$\begin{gathered} y \ = f(x) = (f_1(x), f_2(x), \dots f_n(x)) \\ e(x) = (e_1(x), e_2(x), \dots e_m(x)) \leq 0 \\ x = (x_1, x_2, \dots x_m) \in X,\ y = (y_1, y_2, \dots y_m) \in Y \end{gathered} \tag{8}$$

In general, the multipurpose optimization problem can be described as vector function mapping m parameters to n objectives. In Equation (8), x is a decision vector, X is a parameter space, y is an objective vector, Y is an objective space, and $e(x)$ is a constraint. The set of solutions to the multi-objective optimization problem comprises of the objective vectors that cannot enhance the value of any other function without decreasing the value of an objective function, in addition to all corresponding decision vectors. These vectors are called the Pareto optimal solution. The mathematical definition of Pareto domination can be presented as follows. Assuming a minimization problem and postulating that there are two decision vectors, it can be formulated as Equation (9) [25–27].

$$\forall i \in \{1,\ 2,\ 3,\ \dots,\ n\} : f_i(a) \leq f_i(b) \bigwedge \exists j \in \{1,\ 2,\ 3,\ \dots,\ n\} : f_i(a) \leq f_i(b) \tag{9}$$

A program was created based on the multi-purpose optimization theory described above, and MATLAB (2019, The MathWorks Inc.,Natick, MA, USA), a commercial numerical analysis program, was employed to apply and modify the optimization technique. To optimize the welding process parameters for which brittle fracture characteristics were substantiated, the same 144 data items listed in Table 10 learned in discriminant analysis were used. Furthermore, the variables and levels used to steer the multi-purpose optimization algorithm are shown in Table 13.

Table 13. Multi-objective optimization algorithm parameters and their values.

Optimal Method		MOO (Multi-Objective Optimization)
Range of Local Parameters	L (Laser Power)	$[-0.5 \leq \text{Input} \leq +0.5]$ kW
	D (Defocusing)	$[-0.25 \leq \text{Input} \leq +0.25]$ mm
	S (Welding Speed)	$[-0.15 \leq \text{Input} \leq +0.15]$ m/min
Range of Constraints	H_i (Heat Input)	$H_i \geq 9.16 \times 10^7$ J/cm^2, $H_i \leq 8.22\ 9.16 \times 10^7$ J/cm^2
Fitness Factor	Population Size	50, 60, 70, 80, 90, 100
Solver		Constrained nonlinear minimization
Algorithm		Trust region reflective algorithm
Derivatives		Gradient supplied

A range of fiber laser welding process variables in the multi-purpose optimization algorithm was selected from the minimum (3 kW, −0.5 mm, 0.5 m/min) to the maximum (5 kW, +0.5 mm, 0.8 m/min). Additionally, the brittle fracture characteristics were derived by generating an index, within the selected process variables, that can be used to evaluate the quality deterioration characteristics for 9% Ni steel welds. The objective function is a mathematical model of the problem of an optimization system, and the constraint provides a guide that ensures quality in a range that the system must avoid. Therefore, Equations (10)–(12) represent the objective function $f(x)$ of an arbitrary system with x as a learning variable and the range of constraints required for the function [28].

$$Optimize\ f(L,\ D,\ S) \tag{10}$$

$$g(L,\ D,\ S) \tag{11}$$

$$H_i \geq 9.16E + 07\text{J}/\text{cm}^2,\ H_i \leq 8.22E + 07\text{J}/\text{cm}^2 \tag{12}$$

Based on the multi-purpose optimization algorithm defined above, test Nos. 4, 8, and 17 were chosen to undergo the optimization procedure, in addition to satisfying the limits according to the algorithm flow chart. Table 14 shows the welding process parameters that were amended in the optimization procedure, as well as the envisaged welding factors and groups.

Table 14. Results of welding parameters modified by the optimization process.

Test No.	Original			Modified			Welding Factors				Group
	C	*V*	*S*	*C*	*V*	*S*	*W*	*H*	H_i	*I*	
4	4.0	−5.0	0.5	3.91	−0.51	0.51	5.0	7.7	9.20×10^7	55.6	Dimple
8	5.0	0.0	0.5	5.25	−0.25	0.43	7.9	10.6	9.27×10^7	51.9	Dimple
17	5.0	0.0	0.8	5.23	0.24	0.92	4.7	6.4	7.26×10^7	64.8	Dimple

Figure 11 shows the change in quality characteristics of a weld according to the modified process variables. This demonstrates that it is possible to secure the rigidity of a weld in the vicinity of the process area due to the optimization algorithm function that improves the existing process variables that may cause brittle fracture characteristics and that it has the ability to prevent quality deterioration. In addition, the two raw data items selected from the fiber laser welding process met all of the heat-input-limiting conditions that can cause brittle fracture characteristics. The quality deterioration characteristics evident in the existing process variables were removed by the modified process variables.

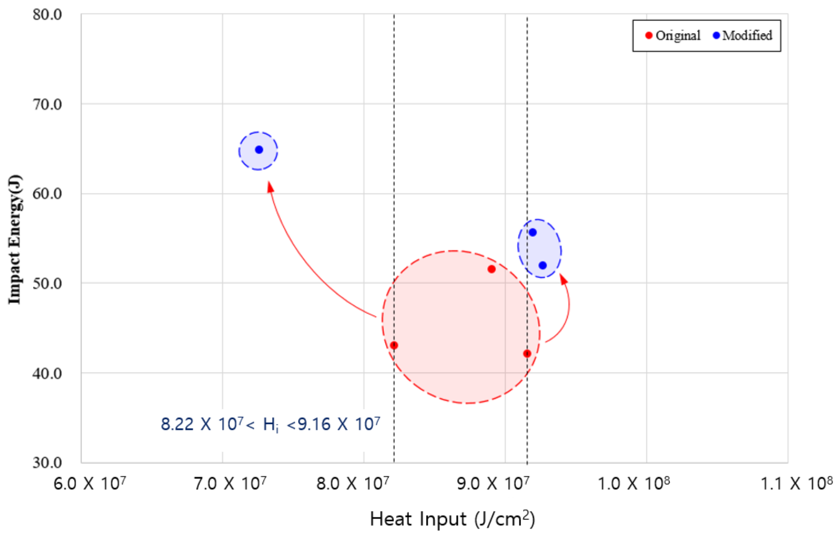

Figure 11. Brittle fracture behavior distributions using modified input parameters.

6. Conclusions

With this study, we attempted to optimize the fiber laser welding process for 9% Ni steel, which is predominantly used to manufacture LNG storage tanks.

(1) An appropriate weld ability was verified by measuring the welding characteristics of a weld obtained from the fiber laser welding experiment, and it was established that the decrease in toughness occurred ((8.22×10^7~9.16×10^7) J/cm^2) due to excessive heat input.
(2) To determine the brittle fracture characteristics of 9% Ni steel according to the welding process variables and the amount of heat applied by a penetration shape, the data of the input and output variables of the welding process were learned through the SVM technique, and it was verified whether a brittle fracture group with deteriorated quality was accurately identified. As a result, it was confirmed that 100% of the group that determined the hardening of the weld could be identified using the learned system.
(3) To optimize the specific welding process parameters with which brittle fracture characteristics occur, a mathematical model that can predict the penetration shape and impact energy was developed and applied to a multipurpose optimization algorithm. After inputting the process variables in the three cases (test Nos. 4, 8, and 17) in which quality degradation occurs, the revised process variables were re-experimented. As a result, the condition for brittle fracture characteristics was eliminated by avoiding the limited heat input section in which the toughness decrease occurred.

Author Contributions: Conceptualization, M.P.; methodology, M.P.; software, C.P.; validation, J.K.; formal analysis, M.P.; investigation, M.P.; resources, J.K.; data curation, M.P.; writing—original draft preparation, M.P.; writing—review and editing: J.K., C.P.; visualization, C.P.; supervision, J.K.; project administration, J.K.; funding acquisition, J.K. All authors have read and agreed to the published version of the manuscript.

Funding: This study was conducted with the support of the Korea Institute of Industrial Technology as "The dynamic parameter control based smart welding system module development for the complete joint penetration weld (KITECH EH-21-0003)".

Institutional Review Board Statement: Not applicable.

Informed Consent Statement: Not applicable.

Data Availability Statement: The data presented in this study are available on request from the corresponding author.

Conflicts of Interest: The authors declare no conflict of interest.

References

1. Assche, R. LNG Bunkering in Europe. Port of Rotterdam Authority. In Proceedings of the 3rd Annual LNG Bunkering Conference, Singapore, 29–31 July 2015.
2. Schinas, O.; Butler, M. Feasibility and commercial considerations of LNG-fueled ships. *Ocean Eng.* **2016**, *122*, 84–96. [CrossRef]
3. Unseki, T. Environmentally Superior LNG-Fueled Vessels. *Mitsubishi Heavy Ind. Tech. Rev.* **2013**, *50*, 37–43.
4. Azzara, A.; Rutherford, D.; Wang, H. Feasibility of IMO annex VI Tier III implementation using selective catalytic reduction. *Int. Counc. Clean Transp.* **2014**, *4*, 1–9.
5. Kim, J.H.; Shim, K.T.; Kim, Y.K.; Ahn, B.W. Fatigue Crack Growth Characteristics of 9% Ni Steel Welded Joint for LNG Storag Tank at Low Temperature. *J. Weld. Join.* **2010**, *28*, 537–542.
6. Lee, S.H.; Lee, S.R.; Lee, Y.S. Interpretation for Band-Type Indication on Radiography of 9% Ni Steel Welds for LNG Storage Tanks. *J. Korean Soc. Nondestruct. Test.* **2010**, *30*, 479–483.
7. Chang, W.S.; Kim, K.C.; Kim, Y.C.; Kim, S.R.; Kim, W.S. Ni alloy welding consumables for 9% Nickel steel. *J. Korean Weld. Soc.* **1998**, *16*, 25–37.
8. R&B Inc. ASTM E23-07 Standard Test Methods for Notched Bar Impact Testing of Metallic Materials. *Am. Soc. Test. Mater.* **2007**, *7*, 1–6.
9. Yun, T.J.; Oh, W.B.; Lee, B.R.; Lee, C.W.; Na, H.H.; Choi, J.S.; Kim, I.S. A Study on Optimization of Fillet in Laser Welding Process for 9% Ni Steel Using Gradient-Based Optimization Algorithm. *J. Weld. Join.* **2020**, *38*, 485–492. [CrossRef]

10. Lee, S.H.; Lee, D.O.; Park, K.S.; Jeon, H.C.; Kim, S.T.; Park, J.U. Laser Welding Deformation Control of STS304 Cylindrical Steel Sheet Structure. *J. Weld. Join.* **2020**, *38*, 521–527. [CrossRef]
11. Go, B.S.; You, H.Y.; Bang, H.S.; Kim, C.H. Penetration Depth Modeling and Process Parameter Maps for Laser Welds Using Machine Learning. *J. Weld. Join.* **2021**, *39*, 392–401. [CrossRef]
12. Welding and bonding hand book—Process and thermal processing. *Int. J. Korean Weld. Soc.* **2007**, *3*, 26–33.
13. El-Shabasy, A.; Lewandowski, J. Effects of load ratio, R, and test temperature on fatigue crack growth of fully pearlitic eutectoid steel (fatigue crack growth of pearlitic steel). *Int. J. Fatigue* **2004**, *26*, 305–309. [CrossRef]
14. Yoon, Y.K.; Kim, J.H.; Shim, K.T. Mechanical Characteristics of 9% Ni Steel Welded Joint for LNG Storage Tank at Cryogenic. *Int. J. Mod. Phys. Con. Ser.* **2012**, *6*, 355–360. [CrossRef]
15. Macek, K. Fracture Surface Formation of Notched 2017A-T4 Aluminium Alloy under Bending Fatigue. *Int. J. Fract.* **2022**, *234*, 141–157. [CrossRef]
16. Tang, W.; Wang, Y. Fractal Characterization of Impact Fracture Surface of Steel. *Appl. Surf. Sci.* **2012**, *258*, 4777–4781. [CrossRef]
17. Ai, Y.; Liu, X.; Huang, Y.; Yu, L. Numerical analysis of the influence of molten pool instability on the weld formation during the high speed fiber laser welding. *Int. J. Heat Mass Transfer* **2020**, *160*, 120103. [CrossRef]
18. Ai, Y.; Yu, L.; Huang, Y.; Liu, X. The investigation of molten pool dynamic behaviors during the "∞" shaped oscillating laser welding of aluminum alloy. *Int. J. Therm. Sci.* **2022**, *173*, 1073507. [CrossRef]
19. Kim, Z.H. A Comparative Study of Classification Techniques Using Forest Cover Type Data: Discriminant Analysis, Logistic Regression, Neural Network, Decision Tree. Unpublished. Master's Thesis, Chung-Ang University, Seoul, Korea, 2012.
20. Amrine, D.E.; White, B.J.; Larson, R.L. Comparison of classification algorithms to predict outcomes of feedlot cattle identified and treated for bovine respiratory disease. *Comput. Electron. Agric.* **2014**, *105*, 9–19. [CrossRef]
21. Knowles, J.D.; Corne, D.W. Approximating the nondominated front using the pareto archived evolution strategy. *Evol. Comput.* **2000**, *8*, 149–172. [CrossRef]
22. Vapnik, V.N. *The Nature of Statistical Learning Theory*; Springer: Berlin/Heidelberg, Germany, 1999.
23. Rheem, I.S.; Rheem, S.S. Response Surface Analysis of the Experimental Data from a Cubic Central Composite Design in the Presence of the Lack of Fit of the Second-Order Polynomial Regression Model. *J. Korean Data Anal. Soc.* **2020**, *22*, 121–129. [CrossRef]
24. Kim, Y.G. *Evolutionary Algorithms*; Chonnam National University Press: Gwangju, Korea, 2011.
25. Deb, K.; Agrawal, S.; Pratap, A.; Meyarivan, T. A fast elitist non-dominated sorting genetic algorithm for multi-objective optimization: NSGA-II. *Lect. Notes Comput. Sci.* **2000**, *1917*, 849–858.
26. Zitzler, E.; Deb, K.; Thiele, L. Comparison of multiobjective evolutionary algorithms: Empirical results. *Evol. Comput.* **2000**, *8*, 173–195. [CrossRef] [PubMed]
27. Veldjuizen, D.A.V.; Lamont, G.B. On measuring multiobjective evolutionary algorithm performance. *Evol. Comput.* **2000**, *1*, 204–211.
28. Deb, K.; Pratap, A.; Agarwal, S.; Meyarivan, T.A. A fast and elitist multi objective genetic algorithm: NSGA-II. *IEEE Trans. Evol. Comput.* **2002**, *6*, 182–197. [CrossRef]